ACS OMEGA

http://pubs.acs.org/journal/acsodf

Article

BASIC: A Comprehensive Model for SO_x Formation Mechanism and Optimization in Municipal Solid Waste (MSW) Combustion

Wenchao Ma, Xu Liu, Chen Ma, Tianbao Gu, and Guanyi Chen*

Cite This: *ACS Omega* 2022, 7, 3860−3871

Read Online

ACCESS | Metrics & More | Article Recommendations | Supporting Information

ABSTRACT: Municipal solid waste (MSW) incineration is one of the main techniques currently used for waste to energy (WTE) conversion in China. Although the sulfur content in MSW is lower than that in coal, its emission cannot be neglected due to environmental pollution, malodor, health problems, and global climate change. Therefore, it is particularly important to effectively predict and control the sulfur pollutants. In this study, a comprehensive model was developed and coupled with the full combustion process bed model bulk accumulated solids incineration code (BASIC) to investigate the formation and transformation processes of sulfur in MSW incineration. The submodels of the four stages in the MSW combustion processes; governing equations of mass, momentum, and energy conservation; and various chemical reactions were included in the model. Based on this model, the effects of different parameters on the formation of sulfur pollutants during the incineration process were studied under different operating conditions. The study finds that for SO_X formation, initial temperature, primary air volume, and material particle size have significant impacts, whereas pressure shows a less significant effect. This article also considers H_2S, COS, and CS_2 formation under different conditions. An optimization study was performed to reduce SO_X pollutants.

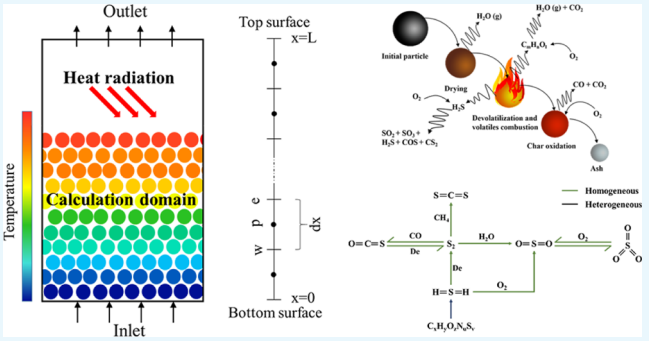

1. INTRODUCTION

The worldwide concern with the rising production of municipal solid waste (MSW) and the limit of fossil fuels have accelerated global interest in waste to energy (WTE) conversion.[1] About 1.3 billion tons of MSW was produced worldwide in 2010 and the global MSW generation is expected to reach 2.2 and 4.2 billion tons by 2025 and 2050, respectively, which could lead to wastage of resources and environmental pollution.[2] As a well-proven and established method for treating MSW, incineration can extract up to 80% of the energy contained in waste and reduce the solid volume by up to 90%.[3,4] Currently, more than 325 million tons of MSW is treated globally in more than 2500 MSW incineration plants with power generation around the world.[5] SO_X emissions are generated from the high-temperature oxidation process of MSW combustion, which is mainly composed of SO_2 and SO_3.[6] The sulfur content of MSW is lower than that of the traditional fossil fuels, but MSW combustion is still one of the major contributors to sulfur pollution. According to the current EU directive on the SO_2 emission limit, the daily average limit is 50 mg/Nm^3 (O_2 content 11%) for MSW incineration plants.[7] However, the daily average limits of SO_2 from WTE plants and coal-fired plants in China are 80 mg/Nm^3 (O_2 content 11%) and 50 mg/Nm^3, respectively. This means SO_2 emission control from WTE plants still needs to be emphasized in the near future.

The release of sulfur under various conditions has been studied in detail by several researchers. Pollutants such as SO_2 and SO_3 are the main sources of acid rain. Up to 10% of SO_2 is converted to SO_3 during combustion.[8] Furthermore, SO_2 and H_2S are the major species during combustion. H_2S is much toxic; even trace amounts of H_2S will have a strong effect on the human respiratory tract and eyes. Another type of sulfur gas CS_2 is produced in combustion and has a low chemical reactivity, but it can be oxidized to SO_2 through photochemical reactions in the atmosphere, which will also cause the formation of acid rain. Therefore, it is necessary to study the formation mechanisms and concentration trends of sulfur species during MSW combustion. However, this study is difficult to investigate in industrial-scale incinerator experiments. In contrast, numerical simulation seems to be an attractive method.

Until now, there are a few studies on the incineration model of sulfur, and most of them are merely based on the kinetics of

Received: July 9, 2020
Accepted: October 5, 2020
Published: January 26, 2022

https://doi.org/10.1021/acsomega.0c03287
ACS Omega 2022, 7, 3860−3871

chemical reactions. Mueller et al. established a chemical reaction kinetic model of SO_X in a fluidized bed reactor, and the simulation results of SO_2 showed that the conversion rate of SO_2 to SO_3 was about 10%.[9] Zarei used a modified reaction kinetic model to describe the generation process of SO_X pollutants in the Claus reaction furnace. He optimized the operating parameters during the waste combustion process and obtained the best-operating conditions such as the initial temperature of the reactor to reduce the COS emissions from waste heat boilers.[10] Ghahraloud et al. established a one-dimensional mathematical model to change the inlet temperature of the fixed bed reactor, the feed rate along with the furnace, and the airflow in the furnace to improve the recovery rate of S and reduce the emission of S-type pollutants. Simulation results show that compared with the conventional process, the S recovery rate is improved by about 4.63%.[11] In addition, Gungor et al. also conducted simulation studies on SO_2 and other gas pollutants produced by coal combustion on a circulating fluid bed. Their results showed that the increase of excess air could reduce SO_2 production and the concentration of SO_2 was lower under the condition of higher inlet pressures.[12]

Although the above researchers have investigated SO_X concentration prediction models based on incineration and simulated SO_X pollutants under different operating conditions, these studies have not explored the transformation process of SO_X pollutants in the gas−solid phase in the incineration bed. They only focused on the gas-phase process and involved relatively less SO_X pollutants and initial operating conditions. A fixed bed reactor is mainly composed of two parts: a packed bed region containing solid waste and gas and a gas-based freeboard region. Commercial computational fluid dynamics (CFD) software such as Fluent can be used to easily simulate the freeboard area. However, accurate modeling of packed bed areas is a challenging part due to the various homogeneous and heterogeneous reactions and corresponding heat- and mass-transfer processes in the boundary area. MSW combustion in the packed bed region is an important part of the incineration process because it is the place where most of the pollutants (SO_X, NO_X, heavy metals, etc.) are generated.[13,14] Therefore, there is a need to study the changing trend of various SO_X gas pollutants in the packed bed region to explore the production of SO_X pollutants under different operating conditions.

To study the generation mechanism and emission characteristics of SO_X and other sulfur pollutants, we took advantage of the most relevant descriptions of early studies. We have developed the bulk accumulated solids incineration code (BASIC) model for simulating the behavior of a burning MSW bed.[15] This model targets the packed bed region and can facilitate the freeboard CFD simulation by providing the inlet conditions from the packed bed region. The model is based on the CFD theory and simulates the overall incineration process within the packed bed, including MSW drying, devolatilization, volatile combustion, and char oxidation processes. To develop a comprehensive model, various operating conditions including pressure, initial temperature, primary airflow rate, and material particle size are taken into account to investigate the effect of these parameters on the formation of different sulfur contaminants (SO_2, SO_3, H_2S, CS_2, COS, S_2). Furthermore, the results predicted by BASIC are validated by comparing with experimental data from the literature, and the formation mechanism of all sulfur species is revealed in detail.

2. MODEL DEVELOPMENT

The model of MSW bed combustion is based on the description of the most actual physical, chemical, and thermal phenomena. The kinetic data of reactions and the equations of energy, momentum, and mass fractions are used to describe these phenomena and calculate the local velocity, pressure, temperature, and composition. Figure 1 shows a conceptual

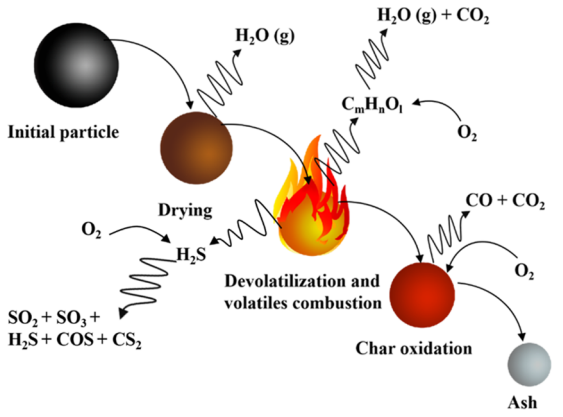

Figure 1. Illustration of different combustion subprocesses of solid waste particle.

view of the combustion process of solid waste particles. It describes the physical, chemical, and thermal reactions of solid waste particles during combustion. The incineration processes are simplified in the following description. First, primary air is injected from the bottom of the reactor. The bed of waste that contains a certain amount of moisture is then heated by the thermal radiation causing the waste on the surface to catch fire from the freeboard; the heated waste undergoes evaporation of water. As the heating continues, the organic matter is decomposed into volatile components, including tar, char, and gases. As the reaction progresses, it will also experience gas combustion and oxidation of the char.[16] During the combustion reaction with oxygen, the heat generated from these reactions will continue to increase the temperature in the packed bed region.[17] When the combustion process is complete, the fixed carbon is consumed, cooled by the air supply, and finally turn into ash.[18,19]

Referring to the MSW incineration process mentioned above, the corresponding chemical reaction equation and chemical reaction kinetic model were determined. Subsequently, the reaction rate was substituted into the source term of Navier−Stokes (N−S) governing equations based on the CFD theory. Finally, according to the physical characteristics of the top and bottom boundaries of the packed bed during the incineration process, the boundary conditions were determined, and the incineration model of the packed bed was established as well. The establishment of the model is described in detail as follows.

2.1. Modeling of the Packed Bed. As a one-dimensional unsteady-state model, BASIC divides the MSW incineration process into four parts, namely, drying, devolatilization, volatiles combustion, and char oxidation. The corresponding chemical reactions and reaction rates of each process are described in Table S1. MSW incineration is a complex physical and chemical process, appropriate assumptions can simplify the simulation process and reduce the amount of calculation, which is inevitable for the simulation work. For the modeling

https://doi.org/10.1021/acsomega.0c03287
ACS Omega 2022, 7, 3860−3871

Table 1. Main Combustion Reactions in the Model

reaction	A	b	E	reaction rate (R_{kin})	refs
$H_2 + 0.5O_2 \rightarrow H_2O_{(g)}$ (R1)	6.8×10^{15}	−1	1.67×10^8	$k[H_2]^{0.25}[O_2]^{1.5}$	18
$CH_4 + 1.5O_2 \rightarrow CO + 2H_2O_{(g)}$ (R2)	5.012×10^{11}	0	2×10^8	$k[CH_4]^{0.7}[O_2]^{0.8}$	30
$CH_4 + H_2O \rightarrow CO + 3H_2$ (R3)	3×10^8	0	1.26×10^8	$k[CH_4][H_2O]$	18
$CO + 0.5O_2 \rightarrow CO_2$ (R4)	2.239×10^{12}	0	1.702×10^8	$k[CO][O_2]^{0.25}[H_2O]^{0.5}$	18
$CO + H_2O \rightarrow CO_2 + H_2$ (R5)	2.75×10^9	0	8.4×10^7	$k[CO][H_2O]$	18

of MSW combustion, six assumptions were made to facilitate the description of this phenomenon: (1) the physical parameters at the same height are consistent with the physical parameters at the center point of the height;[20] (2) MSW is considered as homogeneous porous media;[21] (3) the solid phase and gas phase have the same temperature in the same grid;[22] (4) MSW is considered to be mainly composed of C, H, O, N, and S. The gas species involved in the model are N_2, O_2, CO, CO_2, CH_4, H_2, H_2O, NO, NH_3, HCl, SO_2, SO_3, H_2S, S_2, CS_2, and COS, and the solid species considered are moisture, volatiles, fixed carbon, and ash.[15,19,23] (5) Primary air is injected into the reactor at the bottom of the reactor; (6) the gas is considered to be incompressible and perfect;[24] and (7) the particle size of the MSW particles is constant.

After the drying process, volatile products emerging from the surface of the particles are first mixed with air in the interstices of the particles. Obviously, the combustion of volatile compounds is not only affected by the reaction kinetics (temperature-dependent) but also by the mixed ratio of volatiles to air. The actual volatile combustion reaction rate follows the minimum values of the mixing rate and kinetic rate of the gas phase as follows[25]

$$r = \min(R_{kin}, R_{mix}) \tag{1}$$

The gases are mixed with the surrounding air during combustion; the mixing rate of volatiles under fire can be expressed as follows

$$R_{mix} = C_{mix}\rho_g\left\{150\frac{(1-\phi)^{2/3}D_g}{\phi d_p^2} + 1.75\frac{U_g(1-\phi)^{1/3}}{\phi d_p}\right\} \times \min\left\{\frac{Y_1}{S_1}, \frac{Y_2}{S_2}\ldots\right\} \tag{2}$$

The kinetic constants of the chemical reaction of volatile combustion are shown in Table 1. The reaction rate constant is calculated according to the Arrhenius formula

$$k = AT^b \exp\left(-\frac{E}{RT}\right) \tag{3}$$

2.2. Governing Equations and Boundary Conditions. According to the conservation of energy, mass, and momentum, the governing equations are established for the solid phase and gas phase. They are used to describe the combustion phenomena such as flow, diffusion, and reactions of the solid and gas phases in the calculation region of the packed bed. The heat and mass loss from the top and bottom boundaries are governed by the boundary conditions, and there is no inner heat and mass loss inside the bed. The specific equations are described in Table S2.[26]

In this model (Figure 2), the bottom boundary layer transfers heat and mass to the higher part, and the top boundary surface transfers heat and mass to the freeboard region. Therefore, the boundary conditions are essential for the heat- and mass-transfer process between the packed bed region and the freeboard region.

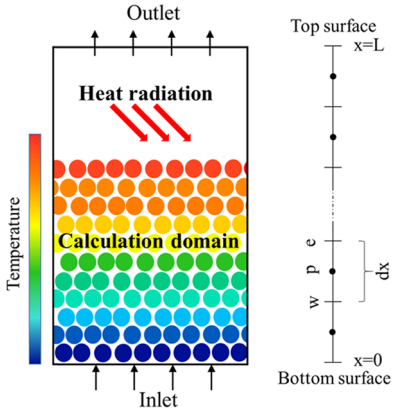

Figure 2. Model computing region and grid division.

At the bottom of the bed, the equation for the temperature is written as follows[15]

$$k_{eff}A\frac{\partial T}{\partial x}|_s = Ah_T(T_\infty - T_s) + A\varepsilon\sigma[T_{rad}^4 - (T_s^*)^4 - 4(T_s^*)^3(T_s - T_s^*)] \tag{4}$$

where T_s^* is the assumed temperature of the boundary layer and is generally set as the initial primary air temperature.

At the bottom of the bed, the concentration of gaseous species at the boundary layer of the fixed bed is obtained from the following equation[15]

$$D_{ig}A\frac{\partial Y_i}{\partial x}|_s = Ah_s(Y_{i,\infty} - Y_{i,s}) \tag{5}$$

At the top surface of the bed, the temperature and gaseous concentrations are governed by equations similar to eqs 4 and 5.

Due to the large difference in the grid density between the boundary layer and the calculation area, the top surface speed needs to be modified as follows

$$u_N \times M_N = u_{N-1} \times M_{N-1} \tag{6}$$

where u_N is the velocity of the top boundary, M_N is the mass of gas out of the layer, and u_{N-1} and M_{N-1} refer to the corresponding factor in the last grid.

2.3. Sulfur Formation Model. This section mainly describes the generation and reaction mechanism of sulfur pollutants and their corresponding chemical reaction kinetic models inside the reactor, laying a foundation for the subsequent prediction of concentration fields of various sulfur gas pollutants. In this model, it mainly involves five sulfur

https://doi.org/10.1021/acsomega.0c03287
ACS Omega 2022, 7, 3860−3871

substances, SO_2, SO_3, H_2S, CS_2, and COS, and eight related chemical reactions, two of which are reversible reactions. The main reaction routes of sulfur species conversion during the combustion are shown in Figure 3.

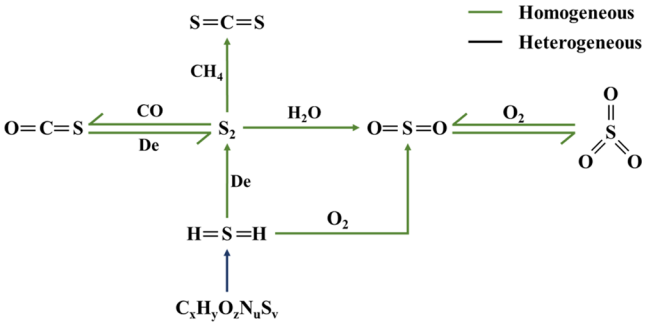

Figure 3. Major routes of sulfur conversion.

Among the main reactions routes, the reactions involving sulfur substances mainly occur in the volatile combustion process of the MSW combustion. First, H_2S gas is produced from the volatilization (pyrolysis) process. Subsequently, one part of H_2S is oxidized in the gas-phase region of the fixed bed to produce SO_2 (R6R6), which is further oxidized to SO_3 (R7R7, R8R8). In addition, as the temperature increases, the other part of H_2S decomposes to S_2 gas (R13R13), and S_2 reacts with CO, CH_4, and H_2O (R9R9−R11) in the gas phase of the bed to generate sulfur gas pollutants such as CS_2 and COS. A sulfur model with eight global homogeneous reactions is introduced in this work, as illustrated in Table 2.

2.4. Solving Method. In the above model description, all of the governing equations are composed of a transient term, a convection term, a diffusion term, and a source term (some equations do not have the convection term and diffusion phase, the correlation coefficient of which can be regarded as 0). Therefore, all of the governing equations can be written into a general equation form as follows

$$\frac{\partial(\rho\Phi)}{\partial t} + \frac{\partial(\rho u\Phi)}{\partial x} = \frac{\partial^2(\lambda\nabla\Phi)}{\partial x^2} + S_\Phi \quad (7)$$

This study uses the finite volume method to divide the entire calculation area into a finite number of volumes, calculates the discrete governing equations for each finite volume, and uses the central difference scheme for the convection term. In this process, the diffusion term is processed with the full implicit algorithm, the source term is processed with the linear treatment, and the governing equation (eq 7) is discretized into the form of a linear matrix. All governing equations are solved through the SIMPLE algorithm.[27]

2.5. Modeling Validation. For the sulfur model developed, the simulation prediction results are compared with the relevant results of the MSW incineration experiment conducted by Tang et al. in a tube furnace to illustrate the accuracy of the established sulfur model.[28] In this experiment, the initial parameters of the treated MSW are shown in Table 3:

The initial parameters of the experiment were inputted into the developed sulfur model. After the debugging and running processes, the relevant simulation results were compared with the results of SO_2 concentration measured in the experiment at 1173 and 1273 K to verify the accuracy of the sulfur model. The comparison results are shown in Figure 4.

Since only SO_2 in SO_X pollutants was studied in the original experiment, this section mainly verified the sulfur model from the perspective of SO_2 production. As shown in Figure 4, the red curve represents the simulation results, while the black curve represents the experimental results. By comparing the production of SO_2 at 1173 and 1273 K, the simulated and experimental results are in good agreement. Hence, the compared results illustrate that the development of the sulfur model has a certain degree of accuracy and it can be used for predicting the SO_X pollutant production during the MSW combustion process.

3. RESULTS AND DISCUSSION

The validated model is used to simulate and predict the main sulfur substances (SO_2, SO_3, H_2S, COS, CS_2) and calculate their production under different working conditions. Furthermore, the variation trend of SO_X pollutants in various working conditions was compared by changing four key parameters in the model: initial temperature, primary air volume, pressure, and material particle size. The simulation results indicate the lowest SO_X production in the MSW combustion process under different conditions so as to achieve the goal of controlling the emission of SO_X pollutants.

3.1. Effect of Temperature on the Concentration of Sulfur Substances. Figure 5 shows the changes of different sulfur substances (SO_2, SO_3, H_2S, COS, CS_2) with time at different initial temperatures (1073, 1173, 1273, 1373 K). It can be appreciated that the model reflects rigorously the strong influence of temperature on the concentration of sulfur substances. This shows that the higher the initial furnace temperature, the faster the reaction rates, which is consistent with the expression of the Arrhenius formula. For SO_2, the

Table 2. Gas-Phase Chemical Reactions Regarding Sulfur Species Introduced into the Model

reaction	A	b	E	reaction rate (R_{kin})	refs
$H_2S + 1.5O_2 \rightarrow SO_2 + H_2O_{(g)}$ (R6)	6.5×10^{14}	0	10 800	$k[H_2S][O_2]$	15
$SO_2 + 0.5O_2 \rightarrow SO_3$ (R7)	9.2×10^{10}	0	8.5×10^5	$k[SO_2][O_2]$	30
$SO_3 \rightarrow SO_2 + 0.5O_2$ (R8)	4.4×10^{11}	0	2.55×10^7	$k[SO_3]$	18
$0.75S_2 + H_2O \rightarrow H_2S + 0.5SO_2$ (R9)	31 081	0	35 564	$k[S_2]^{0.75}[H_2O]$	18
$CH_4 + 2S_2 \rightarrow CS_2 + 2H_2S$ (R10)	5.53×10^{10}	0	19 320	$k[S_2][CH_4]$	18
$CO + 0.5S_2 \rightarrow COS$ (R11)	$3.18 \times 10^{5.}$	0	55 800	$k[S_2][CO]$	15
$COS \rightarrow CO + 0.5S_2$ (R12)	4.36×10^9	0	1.8×10^5	$k[COS]$	31
$H_2S \rightarrow H_2 + 0.5S_2$ (R13)	3.6×10^8	0	2.01×10^5	$k[H_2S]$	31

https://doi.org/10.1021/acsomega.0c03287
ACS Omega 2022, 7, 3860−3871

Table 3. Initial Parameters of the Raw Material

proximate analysis (wt %)				ultimate analysis (wt %)				
moisture	volatile	fixed carbon	Ash	C	H	O	N	S
3.57	73.33	12.64	10.46	41.37	7.10	34.22	1.37	1.94

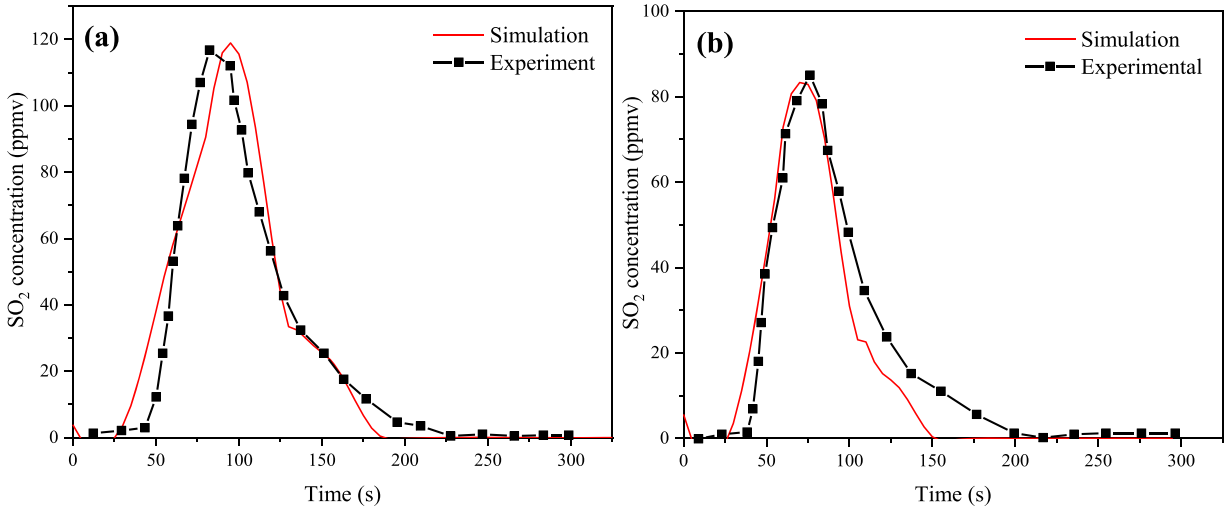

Figure 4. Comparison of simulation and experimental profiles:[28] (a) SO_2 concentration (1173 K) and (b) SO_2 concentration (1273 K).

higher the initial temperature, the lower the production. The peak concentration of SO_2 decreases from 158 ppmv at 1073 K to 60 ppmv at 1373 K with a total decrease of 60 ppmv. This shows that the increasing initial temperature has a significant effect on reducing the SO_2 formation. In addition, it can be seen from Figure 5b that the production of SO_3 also shows a similar trend to that found for SO_2. The peak concentration of SO_3 decreases from 125 ppmv at 1073 K to 20 ppmv at 1373 K with a total decrease of 105 ppmv.

Moreover, as the main sulfur substance, the production concentration peak of H_2S increases with an increase of temperature. The peak concentration of H_2S increases from 700 ppmv at 1073 K to 1150 ppmv at 1373 K with a high increase of 450 ppmv. However, with a further increase of temperature, the shortening of its release time becomes more and more limited. It can be seen that although the temperature can reduce the production of SO_2 and SO_3, it can as well cause an increase in the release of H_2S. Nonetheless, as the temperature gradually increases, the increasing trend of H_2S becomes slower, and its release time becomes shorter.

Finally, for COS and CS_2, the overall change trend gradually increases with increasing temperature; it can be seen that the production of COS and CS_2 also shows a similar trend that can be found in H_2S. The peak concentration of COS and CS_2 increases from 35 and 9 ppmv at 1073 K to 72 and 18 ppmv at 1373 K with a high increase of 450 ppmv, respectively, increasing by 37 and 9 ppmv. As observed, the increasing temperature not only advances the overall incineration reaction but also promotes the transformation of S_2 to COS and CS_2.

3.2. Effect of Pressure on the Concentration of Sulfur Species. Because the total density of the mixed gas changes with pressure, it can be known from the ideal gas formula that the higher the pressure, the greater the density of the gas. In this model, the total density of the mixed gas is updated by the ideal gas formula, so it is particularly important to study the pressure change during the entire bed incineration process. In addition, low pressure exists in many high-altitude areas in China (such as Tibet), so it is of practical significance to study the incineration under different pressures, especially for the MSW incineration characteristics under low pressure in plateau areas. Figure 6 presents the predicted overall concentration of sulfur species in the fixed bed as a function of time with different pressures (91.3, 101.3, 111.3 KPa). As illustrated in Figure 6a,c, when the pressure increases, the concentrations of SO_2 and H_2S change slightly, while the production of SO_3, COS, and CS_2 shows an upward trend with an increase of pressure, increasing by 10, 27, and 4 ppmv, respectively. The main reason for the results is that the molecular diffusion coefficient D_g of the gas is affected by the pressure, and its value increase with pressure. The mixture reaction rate R_{mix} is positively related to the molecular diffusion coefficient D_g of the gas (eq 2). From eq 1, when the value of R_{mix} is less than the kinetic reaction rate R_{kin}, the reaction rate is determined by R_{mix}. Thus, when the reaction rate increases along with pressure, the reaction rates of R7, R10, and R11 determined by R_{mix} increase as well. Therefore, the production of SO_3, COS, and CS_2 increases at high pressures. As for the reactions that are mainly controlled by temperature, the value of R_{kin} is smaller than R_{mix}, so the reaction (R7, R9, R10, R13) rate is mainly affected by R_{kin} and the impact of pressure on SO_2 and H_2S production is relatively small.

3.3. Effect of Particle Size on the Concentration of Sulfur Species. This section mainly simulates the changes of various sulfur gas pollutants under the condition of different average particle sizes (40, 50, 60 mm). As shown in Figure 7a, when the average particle size is 40 mm, the peak concentration of SO_2 is 95 ppmv and it is generated at around 170 s. With an increase of the particle size to 60 mm, the peak concentration increase to 152 ppmv, increasing by 58%, but the generation time is shortened to 150 s. Similarly, for SO_3, when the particle size is 40 mm, its concentration is only 40 ppmv, but with an increase of the particle size, its peak concentration eventually becomes 100 ppmv, increasing by more than twice. As observed, an increase in the particle size

https://doi.org/10.1021/acsomega.0c03287
ACS Omega 2022, 7, 3860−3871

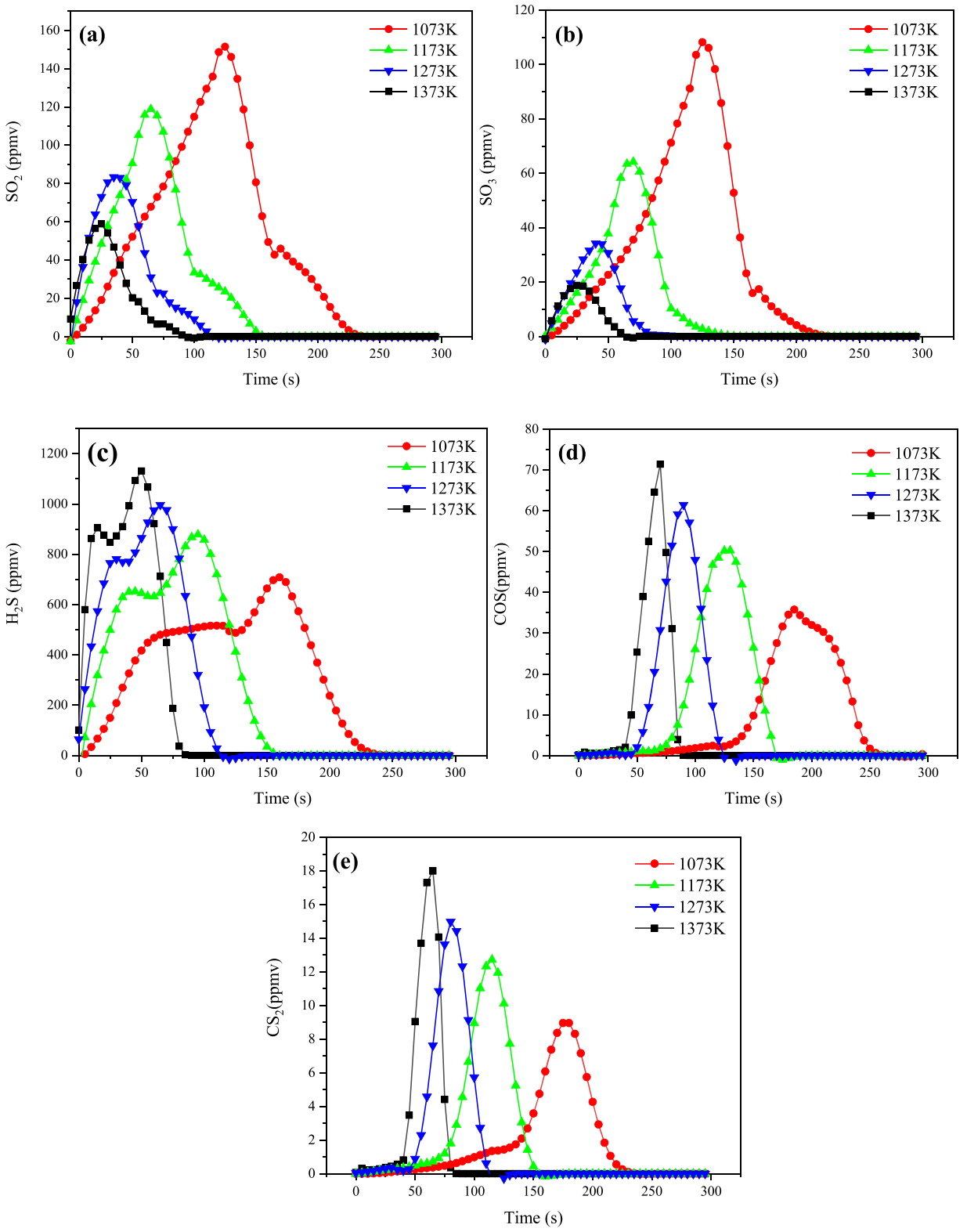

Figure 5. Simulation of different sulfur species (a) SO_2, (b) SO_3, (c) H_2S, (d) COS, and (e) CS_2 concentration overtime at different initial temperatures (1073, 1173, 1273, 1373 K).

has a greater impact on the generation of SO_3. The increase of the peak concentrations of SO_2 and SO_3 is mainly because the heat transfer between the gas phase and the solid phase in the incinerator bed plays a significant role in the generation of NO when the average particle size increases from 40 to 60 mm. The heat transfer between the gas and solid phases in the fixed bed has a significant effect on the formation of SO_X. With an increase in the particle size, the heat transfer between the gas phase and the solid phase in the bed increases, the reaction time advances, and the burning rate of the bed increases, which affects the temperature of the bed and leads to an increase in the concentrations of SO_2 and SO_3.[29] Therefore, SO_2 and SO_3

https://doi.org/10.1021/acsomega.0c03287
ACS Omega 2022, 7, 3860−3871

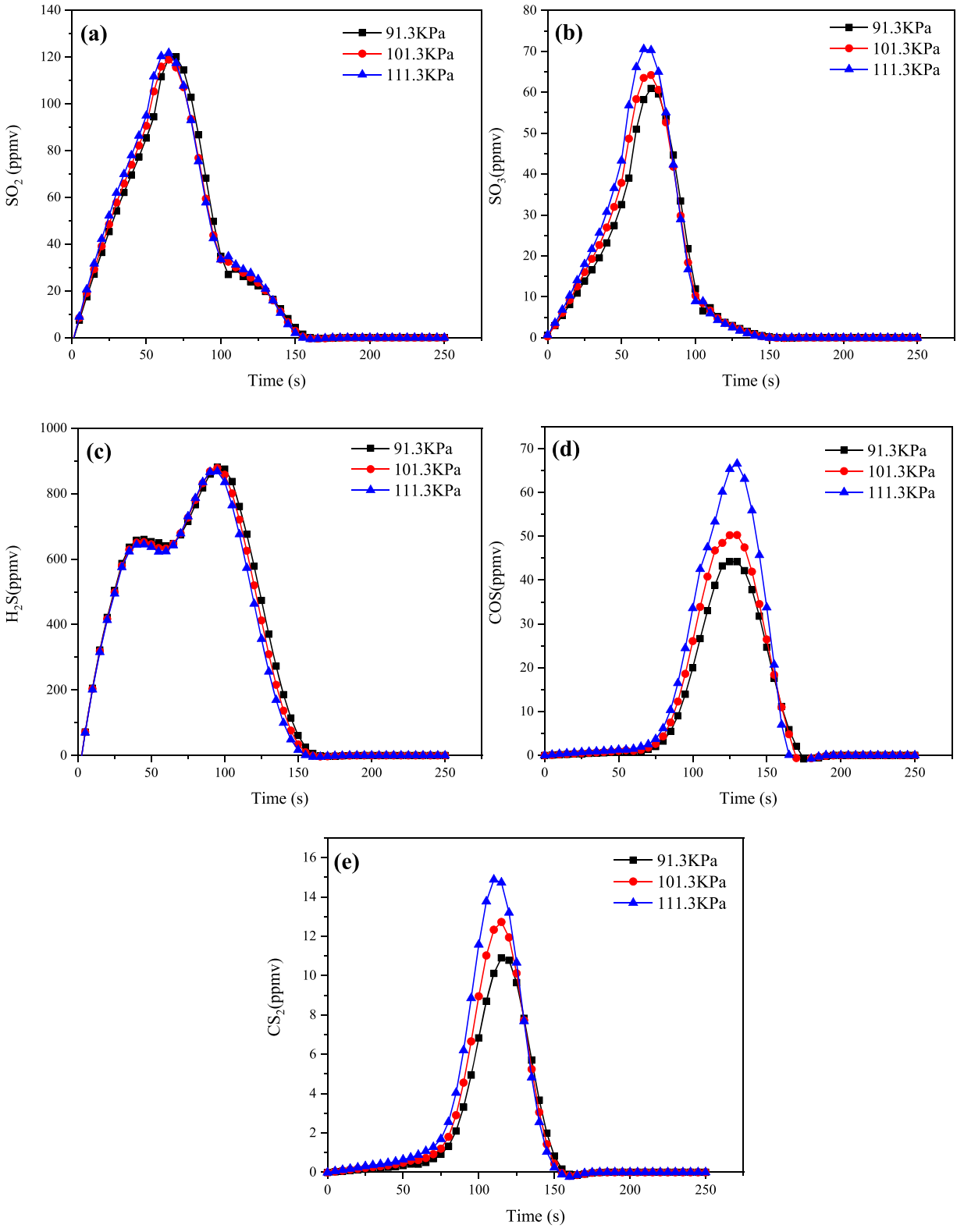

Figure 6. Changes of different sulfur species (a) SO_2, (b) SO_3, (c) H_2S, (d) COS, and (e) CS_2 over time under different pressures.

generated in the packed bed region increase when the average particle size increases from 40 to 60 mm.

For H_2S, Figure 7c shows that the changes in the particle size have less effect on the amount of H_2S produced; however, when particle size increased from 40 to 60 mm, the concentration of the peak value increased from 580 to 700 ppmv. This shows that the increasing particle size facilitates the occurrence of the volatile pyrolysis process, which leads to a higher level of H_2S released into the gas phase. Finally, for the other two substances COS and CS_2, their total production has also increased with an increase in the particle size. Their production increased from 43 to 60 ppmv and from 10 to 15 ppmv, respectively. The increasing trend with the particle size can also be attributed to an increase of heat transfer between

https://doi.org/10.1021/acsomega.0c03287
ACS Omega 2022, 7, 3860−3871

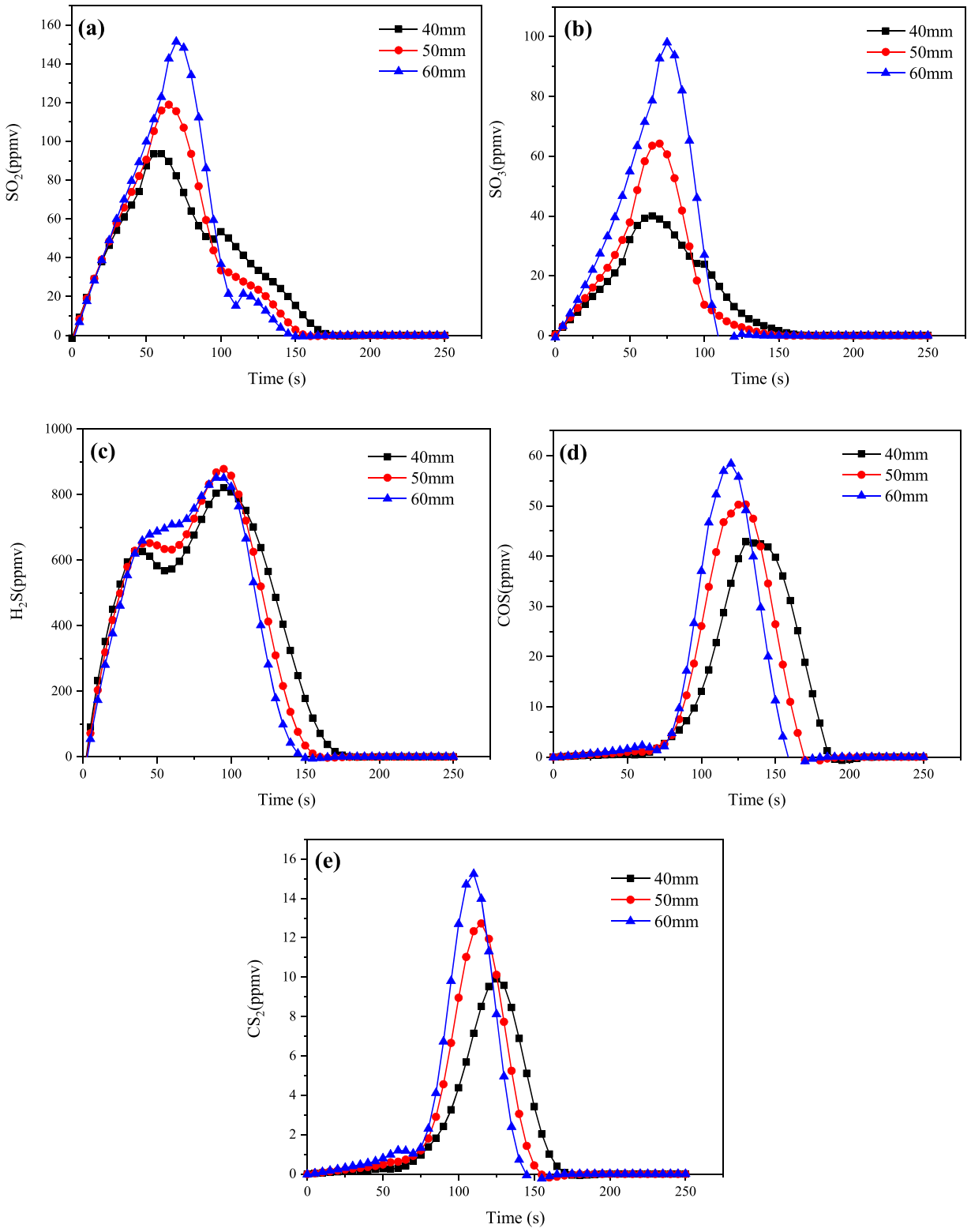

Figure 7. Changes of different sulfur species (a) SO_2, (b) SO_3, (c) H_2S, (d) COS, and (e) CS_2 over time under different particle sizes (40, 50, 60 mm).

solid and gas phases in the packed bed region, which promotes the homogeneous reaction on the bed and thus results in an increase of the related gas product production.

3.4. Effect of Primary Airflow on the Concentration of Sulfur Species. Since the primary air volume can affect the redox atmosphere in the system and thus affect the generation of various gas-phase products, this study also stimulates the generation of sulfur substances under different primary air volumes. As shown in Figure 8, the changes of SO_2, SO_3, H_2S, COS, and CS_2 generation are simulated under the conditions of different primary airflows (0.04, 0.05, and 0.06 kg/(m^3 s)). Figure 8a shows that when the air volume increases to 0.04 kg/

https://doi.org/10.1021/acsomega.0c03287
ACS Omega 2022, 7, 3860−3871

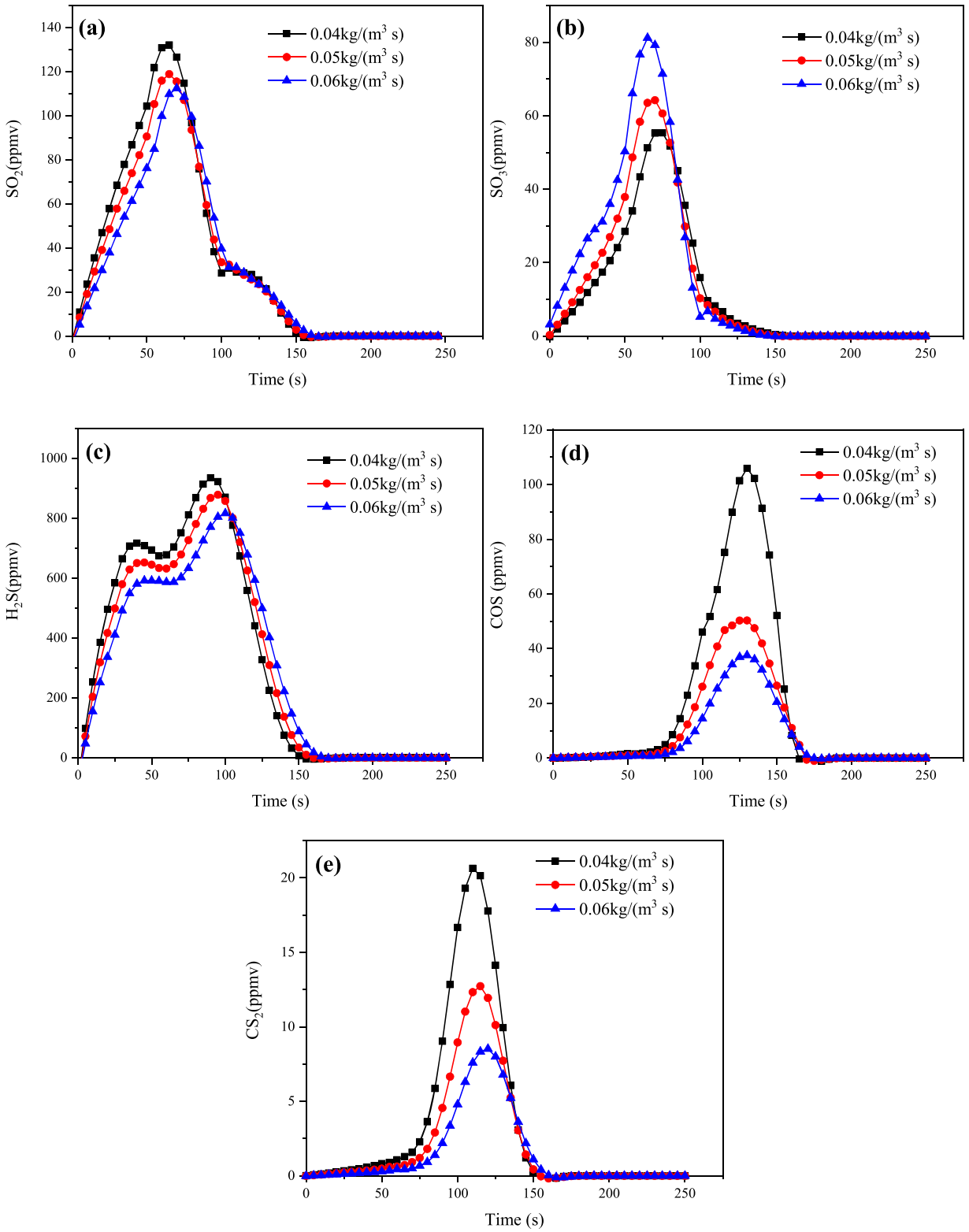

Figure 8. Changes of different sulfur species (a) SO_2, (b) SO_3, (c) H_2S, (d) COS, and (e) CS_2 over time under different primary airflows (0.04, 0.05, 0.06 kg/(m^3 s)).

(m^3 s), the peak value of the SO_2 concentration is 135 ppmv. As the air volume further increases to 0.06 kg/(m^3 s), the peak concentration of SO_2 gradually decreases to 112 ppmv. Therefore, it can be predicted that as the increase of SO_2 in the air gradually convert into SO_3, the increase of the primary airflow will enhance the content of N_2 and O_2 in the system and play the role of air volume to dilute SO_2. In addition, Figure 8b shows that the peak concentration of SO_3 increased from 54 ppmv at 0.04 kg/(m^3 s) to 81 ppmv at 0.06 kg/(m^3 s), which has a total increase of about 50%. Therefore, the simulation further demonstrates that SO_2 in the packed bed

https://doi.org/10.1021/acsomega.0c03287
ACS Omega 2022, 7, 3860−3871

region will be converted into SO_3 at a higher primary air volume, which results in a surge in its peak concentration.

For COS and CS_2 as well, their total production decreases significantly with an increase of primary air volume in the system. The peak concentration of COS decreases from 110 ppmv at the beginning of 0.04 kg/(m^3 s) to 39 ppmv at the end of 0.06 kg/(m^3 s), and the peak concentration of CS_2 decreases from 21 ppmv at the beginning of 0.04 kg/(m^3 s) to 8 ppmv at the end of 0.06 kg/(m^3 s), with decreases of 65 and 62%, respectively. It can be seen that an increase of primary airflow significantly inhibits the generation of these two trace substances and inhibits the transformation of S_2 to COS and CS_2 in the gas phase.

4. CONCLUSIONS

Based on the self-developed one-dimensional unsteady-state bed model BASIC, sulfur chemistry is added to BASIC to predict the concentration of sulfur substances in the fixed bed region under different operating conditions including initial temperatures, pressures, particle sizes, and primary airflow conditions. The formation of sulfur species was discussed from the perspective of the chemical reaction mechanism.

1. At different initial temperatures (1073, 1173, 1273, 1373 K), the production of SO_2 and SO_3 decreased by 98 and 105 ppmv, respectively, showing a significant downward trend, while the peak concentrations of H_2S, COS, and CS_2 showed an increasing trend by 450, 37, and 9 ppmv, respectively.
2. For different average particle sizes (40, 50, 60 mm), the production of SO_2, SO_3, COS, and CS_2 gradually increased with an increase of the particle size, especially for SO_3. The main reason is that the heat transfer between the gas phase and the solid phase in the bed increases with an increase of particle size and the reaction time is advanced, which affects the temperature and leads to the change of its production.
3. For different primary airflows (0.04, 0.05, 60 kg/(m^2 s)), the production of SO_3 increases with an increase of primary air volume, while the other products SO_2, H_2S, COS, and CS_2 show a downward trend with an increase of primary air volume due to the enhancement of an oxidizing atmosphere in the system and the dilution effect of sulfur substances.
4. The suggested optimal operating condition was found to have an initial temperature of 1373 K, a feedstock particle size of 40 mm, and a higher primary airflow rate of 0.06 kg/(m^2 s). Pressure has no significant influence on nitrogen species formation.

According to the simulation results, the model reasonably well predicts the major sulfur species. The optimum parameters for the lowest SO_x production in fixed bed combustion, such as temperature and particle size, can be also predicted. Through the simulation study, the real effects of optimum parameters on the combustion characteristics can be more fundamentally investigated and the direction can be provided for the design and optimization of the MSW fixed bed.

ASSOCIATED CONTENT

Supporting Information

The Supporting Information is available free of charge at https://pubs.acs.org/doi/10.1021/acsomega.0c03287.

Main combustion processes in the model (Table S1) and governing equations in the model (Table S2) (PDF)

AUTHOR INFORMATION

Corresponding Author

Guanyi Chen − *Tianjin Key Lab of Biomass Waste Utilization, School of Environmental Science and Engineering, Key Laboratory of Efficient Utilization of Low and Medium Grade Energy (Ministry of Education), Tianjin University, Tianjin 300072, China; School of Science, Tibet University, Lhasa 850012, China*; Phone: +86-18622639273; Email: chen@tju.edu.cn; Fax: +86-022-8740-1929

Authors

Wenchao Ma − *Tianjin Key Lab of Biomass Waste Utilization, School of Environmental Science and Engineering, Key Laboratory of Efficient Utilization of Low and Medium Grade Energy (Ministry of Education), Tianjin University, Tianjin 300072, China;* orcid.org/0000-0003-3895-5163

Xu Liu − *Tianjin Key Lab of Biomass Waste Utilization, School of Environmental Science and Engineering, Key Laboratory of Efficient Utilization of Low and Medium Grade Energy (Ministry of Education), Tianjin University, Tianjin 300072, China*

Chen Ma − *Tianjin Key Lab of Biomass Waste Utilization, School of Environmental Science and Engineering, Key Laboratory of Efficient Utilization of Low and Medium Grade Energy (Ministry of Education), Tianjin University, Tianjin 300072, China*

Tianbao Gu − *Tianjin Key Lab of Biomass Waste Utilization, School of Environmental Science and Engineering, Key Laboratory of Efficient Utilization of Low and Medium Grade Energy (Ministry of Education), Tianjin University, Tianjin 300072, China; Department of Energy Technology, Aalborg University, DK-9220 Aalborg East, Denmark*

Complete contact information is available at: https://pubs.acs.org/10.1021/acsomega.0c03287

Notes

The authors declare no competing financial interest.

ACKNOWLEDGMENTS

This work was supported by the National Key R&D Program of China [2018YFC1901305], the National Science Foundation of China [51776139, 51676138, and 51878557], and the High Technology Support Project of Tianjin [18ZXSZSF00120].

NOMENCLATURES

A_v	pre-exponent factor (s^{-1})
A_s	solid particle surface area (m^2)
b	temperature order
C_{pg}	gas specific heat capacity (J/(kg K))
C_{pM}	heat capacity of biomass (J/(kg K))
C_{pc}	heat capacity of char (J/(kg K))
C_{pw}	heat capacity of water (J/(kg K)), 4.18
C_{mix}	empirical constant of gas mixture, 0.5
$C_{w,g}$	moisture concentration in the gas phase (kg/m^3)
$C_{w,s}$	moisture concentration on the solid surface (kg/m^3)
D_{ig}	gas diffusion coefficient (m^2/s)

https://doi.org/10.1021/acsomega.0c03287
ACS Omega 2022, 7, 3860−3871

d_p solid particle diameter (m)
E activation energy (J/kmol)
H bed height (mm)
h_{rs} effective radiation heat transfer coefficient of the solid surface (m/s)
h_{rv} effective radiation heat transfer coefficient of the voids (m/s)
h_s convective mass transfer coefficient (m/s)
h_T heat transfer coefficient (W/(m^2 K))
K bed permeability
k_{eff} effective thermal conductivity (W/(m K))
$k_{eff,0}$ effective thermal conductivity without flow (W/(m K))
k_g gas thermal conductivity (W/(m K))
k_r rate constant due to chemical kinetics (kg/atm (m^2 s))
k_d rate constant due to diffusion (kg/atm (m^2 s))
k_{air} air thermal conductivity (W/(m K))
k_s solid thermal conductivity (W/(m K))
M_i i species molar weight (kg/kmol)
ls equivalent thickness of the computed fluid layer (m)
LHV fuel low heating value (kJ/kg)
Nu Nusselt number
P gas pressure (Pa)
P_{O2} oxygen pressure in the gas phase (Pa)
P_r Planck number
Q_{cr} heat absorbed by the solids (W/m^3)
R universal gas constant (J/(mol K)), 8.314
R_c char burnout rate (kg/s)
R_{evp} moisture evaporation rate (kg/s)
r reaction rate (kg/(m^3 s))
Re Reynolds number
R_{kin} kinetic rate of the gas phase (kg/(m^3 s))
R_{mix} mixing rate of the gas phase (kg/(m^3 s))
R_v devolatilization rate (kg/s)
S_a specific area (m^2/m^3)
Sc Schmidt number
Sh Sherwood number
S_g conversion rate from solid to gas (kg/(m^3 s))
S_i corresponding stoichiometric coefficients
S_{ig} source term of the gas species equation (kg/(m^3 s))
S_{is} source term of the solid species equation (kg/(m^3 s))
S_T source term of the energy equation (J/(m^3 s))
S_Φ general source term
t time (s)
T temperature (K)
T_{rad} radiation temperature (K)
T_s temperature of the bed surface (K)
T_∞ the freeboard temperature (K)
U gas velocity (m/s)
V volume of each cell at the current time (m^3)
V_0 volume of each cell at the previous time (m^3)
x_M moisture conversion ratio
x_V volatile conversion ratio
x_C char conversion ratio
Y_w mass fraction of water
Y_c mass fraction of fixed carbon
Y_v mass fraction of gas species
Y_i mass fraction of reactants
Y_{ig} mass fraction of gas species
Y_{air} mass fraction of air
$Y_{i,\infty}$ mass fraction of gas in the freeboard

GREEK LETTERS

β drag force coefficient
β_M shrinking factor of drying
β_V shrinking factor of devolatilization
β_C shrinking factor of char oxidation
Δl characteristic distance between two particles (m)
ε solid emissivity 0.8
σ Boltzmann constant (W/(m^2 K^4)), 5.67 × 10^{-8}
μ dynamic viscosity (Pa s)
ρ_g gas density (kg/m^3)
ρ_s solid bulk density (kg/m^3)
ρ_{is} bulk density of i solids composition (kg/m^3)
σ_i collision diameter (Å)
ϕ bed void fraction, 0.65

REFERENCES

(1) Milutinović, B.; Stefanović, G.; Đekić, P. S.; Mijailović, I.; Tomić, M. Environmental assessment of waste management scenarios with energy recovery using life cycle assessment and multi-criteria analysis. *Energy* **2017**, *137*, 917−926.
(2) Islam, K. M. N. Municipal solid waste to energy generation: An approach for enhancing climate co-benefits in the urban areas of Bangladesh. *Renewable Sustainable Energy Rev.* **2018**, *81*, 2472−2486.
(3) Teixeira, S.; Monteiro, E.; Silva, V.; Rouboa, A. Prospective application of municipal solid wastes for energy production in Portugal. *Energy Policy* **2014**, *71*, 159−168.
(4) Wang, Y.; Zhang, X.; Liao, W.; Wu, J.; Yang, X.; Shui, W.; Deng, S.; Zhang, Y.; Lin, L.; Xiao, Y.; Yu, X.; Peng, H. Investigating impact of waste reuse on the sustainability of municipal solid waste (MSW) incineration industry using emergy approach: A case study from Sichuan province, China. *Waste Manage.* **2018**, *77*, 252−267.
(5) Glushkov, D.; Paushkina, K.; Shabardin, D.; Strizhak, P.; Gutareva, N. Municipal solid waste recycling by burning it as part of composite fuel with energy generation. *J. Environ. Manage.* **2019**, *231*, 896−904.
(6) Sharma, G.; Sinha, B.; Pallavi; Hakkim, H.; Chandra, B. P.; Kumar, A.; Sinha, V. Gridded Emissions of CO, NOx, SO2, CO2, NH3, HCl, CH4, PM2.5, PM10, BC, and NMVOC from Open Municipal Waste Burning in India. *Environ. Sci. Technol.* **2019**, *53*, 4765−4774.
(7) Union T. E. P. A.. Directive 2010/75/EU of the European Parliament and of the council of 24 November 2010 on industrial emissions (integrated pollution prevention and control). *Off. J. Eur. Union* **2010**, *334*, 17−119.
(8) Chen, L.; Bhattacharya, S. Sulfur Emission from Victorian Brown Coal Under Pyrolysis, Oxy-Fuel Combustion and Gasification Conditions. *Environ. Sci. Technol.* **2013**, *47*, 1729−1734.
(9) Mueller, M. A.; Yetter, R. A.; Dryer, F. L. Kinetic modeling of the CO/H2O/O2/NO/SO2 system: Implications for high-pressure fall-off in the SO2 + O(+M) = SO3(+M) reaction. *Int. J. Chem. Kinet.* **2000**, *32*, 317−339.
(10) Zarei, S. Life cycle assessment and optimization of Claus reaction furnace through kinetic modeling. *Chem. Eng. Res. Des.* **2019**, *148*, 75−85.
(11) Ghahraloud, H.; Farsi, M.; Rahimpour, M. R. Modeling and optimization of an industrial Claus process: Thermal and catalytic section. *J. Taiwan Inst. Chem. Eng.* **2017**, *76*, 1−9.
(12) Glarborg, P. Hidden interactions-Trace species governing combustion and emissions. *Proc. Combust. Inst.* **2007**, *31*, 77−98.
(13) Lin, X.; Chen, Z.; Lu, S.; Zhang, S.; Zhang, M.; Li, X.; Yan, J. Emission Characteristics of Polychlorinated Dibenzo-p-dioxins and Dibenzofurans from the Co-combustion of Municipal Solid Waste in a Lab-Scale Drop-Tube Furnace. *Energy Fuels* **2018**, *32*, 5396−5404.
(14) Lin, F.; Wang, Z.; Zhang, Z.; He, Y.; Zhu, Y.; Shao, J.; Yuan, D.; Chen, G.; Cen, K. Flue gas treatment with ozone oxidation: An overview on NO, organic pollutants, and mercury. *Chem. Eng. J.* **2020**, *382*, No. 123030.
(15) Gu, T.; Yin, C.; Ma, W.; Chen, G. Municipal solid waste incineration in a packed bed: A comprehensive modeling study with experimental validation. *Appl. Energy* **2019**, *247*, 127−139.

https://doi.org/10.1021/acsomega.0c03287
ACS Omega 2022, 7, 3860−3871

(16) Hosseini Rahdar, M.; Nasiri, F.; Lee, B. A Review of Numerical Modeling and Experimental Analysis of Combustion in Moving Grate Biomass Combustors. *Energy Fuels* **2019**, *33*, 9367−9402.
(17) Guo, X.; Wang, Z.; Li, H.; Huang, H.; Wu, C.; Chen, Y.; Li, B. A Study on Combustion Characteristics and Kinetic Model of Municipal Solid Wastes. *Energy Fuels* **2001**, *15*, 1441−1446.
(18) Van der Lans, R. P.; Pedersen, L. T.; Jensen, A.; Glarborg, P.; Dam-Johansen, K. Modelling and experiments of straw combustion in a grate furnace. *Biomass Bioenergy* **2000**, *19*, 199−208.
(19) Shin, D.; Choi, S. The combustion of simulated waste particles in a fixed bed. *Combust. Flame* **2000**, *121*, 167−180.
(20) Asthana, A.; Ménard, Y.; Sessiecq, P.; Patisson, F. Modeling On-Grate MSW Incineration with Experimental Validation in a Batch Incinerator. *Ind. Eng. Chem. Res.* **2010**, *49*, 7597−7604.
(21) Goh, Y. R.; Yang, Y. B.; Zakaria, R.; Siddall, R. G.; Nasserzadeh, V.; Swithenbank, J. Development of an Incinerator Bed Model for Municipal Solid Waste Incineration. *Combust. Sci. Technol.* **2001**, *162*, 37−58.
(22) Lu, H.; Robert, W.; Peirce, G.; Ripa, B.; Baxter, L. L. Comprehensive Study of Biomass Particle Combustion. *Energy Fuels* **2008**, *22*, 2826−2839.
(23) Deng, N.; Zhang, A.; Zhang, Q.; He, G.; Cui, W.; Chen, G.; Song, C. Simulation analysis and ternary diagram of municipal solid waste pyrolysis and gasification based on the equilibrium model. *Bioresour. Technol.* **2017**, *235*, 371−379.
(24) Yin, C.; Kær, S. K.; Rosendahl, L.; Hvid, S. L. Co-firing straw with coal in a swirl-stabilized dual-feed burner: Modelling and experimental validation. *Bioresour. Technol.* **2010**, *101*, 4169−4178.
(25) Yang, Y. B.; Yamauchi, H.; Nasserzadeh, V.; Swithenbank, J. Effects of fuel devolatilisation on the combustion of wood chips and incineration of simulated municipal solid wastes in a packed bed☆. *Fuel* **2003**, *82*, 2205−2221.
(26) Yin, C.; Yan, J. Oxy-fuel combustion of pulverized fuels: Combustion fundamentals and modeling. *Appl. Energy* **2016**, *162*, 742−762.
(27) Asako, Y.; Sharma, M. Modification of SIMPLE algorithm to handle supercritical natural circulation in a loop. *Int. J. Heat Mass Transfer* **2018**, *126*, 425−431.
(28) Tang, Y.; Ma, X.; Lai, Z.; Zhou, D.; Lin, H.; Chen, Y. NOx and SO2 emissions from municipal solid waste (MSW) combustion in CO2/O2 atmosphere. *Energy* **2012**, *40*, 300−306.
(29) Sun, R.; Ismail, T. M.; Ren, X.; El-Salam, M. A. Influence of simulated MSW sizes on the combustion process in a fixed bed: CFD and experimental approaches. *Waste Manage.* **2016**, *49*, 272−286.
(30) Zhou, H.; Jensen, A. D.; Glarborg, P.; Jensen, P. A.; Kavaliauskas, A. Numerical modeling of straw combustion in a fixed bed. *Fuel* **2005**, *84*, 389−403.
(31) Zarei, S.; Ganji, H.; Sadi, M.; Rashidzadeh, M. Kinetic modeling and optimization of Claus reaction furnace. *J. Nat. Gas Sci. Eng.* **2016**, *31*, 747−757.

https://doi.org/10.1021/acsomega.0c03287
ACS Omega 2022, 7, 3860−3871